

Least-squares reverse time migration for the Cascadia ocean-bottom dataset

Mandy Wong, Shuki Ronen, and Biondo Biondi

ABSTRACT

We present a method based on least-squares reverse time migration (LSRTM) for imaging ocean-bottom data. We show that by using LSRTM, we not only enhance the resolution of the image but also suppress the migration artifacts. Furthermore, LSRTM also raise the relative amplitude of true reflectors in the subsurface. This method can also be extended to imaging with higher-order multiples. In certain geometries, LSRTM with multiples can further improve the image with a larger aperture. We demonstrate the concept and methodology in 2D and apply our proposed scheme to an ocean-bottom field survey located in the northern Cascadia continental margin.

INTRODUCTION

Ocean-bottom seismic (OBS) acquisition is an established technology in which seismometers are placed on the sea bottom and shots are fired at the sea surface. In areas congested by platforms or other obstacles, ocean-bottom seismic is advantageous, because it is operated by small boats without cumbersome towed streamers.

There are several different processing schemes for ocean-bottom data. The traditional method, inherited from surface seismic processing, is to remove all free-surface multiples and to migrate only with the primary signal (Wang et al., 2009). Therefore, initial work on OBS data processing has been dedicated to the removal of free-surface multiples.

While multiples are often treated as noise, they are formed by the same source signal as primaries, but travel along different paths in the medium. The receiver ghost, also known as the mirror signal, is the next order of reflection beyond the primaries, with an additional reflection off the sea surface. For a deep water OBS survey, the subsurface reflection point of the receiver ghost is located at a greater distance from the receiver station than the primary (Figure 1). Therefore, the mirror signal can provide wider subsurface illumination than the primaries. Several authors have used the mirror signal in migrating OBS data (Godfrey et al., 1998; Ronen et al., 2005; Grion et al., 2007; Dash et al., 2009).

While mirror imaging can greatly expand the illumination aperture of an OBS survey, a similar concept can be applied to image with even higher-order surface-related multiples. Figure 1 shows that the subsurface reflection point of the next

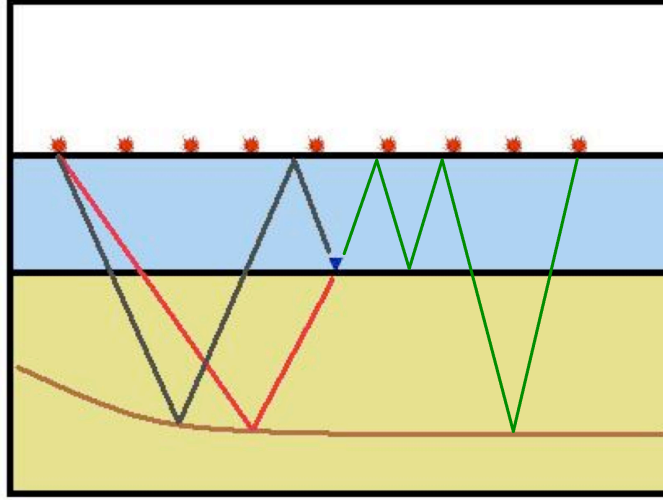


Figure 1: The subsurface reflection point of the double-mirror signal (in green double-line), the mirror signal (in black dashed-line), and the primary signal (in red solid-line). Note the double mirror image point is located at a greater distance from the receiver station than the mirror signal and the primary. [NR]

order of surface-related multiples, denoted as the double-mirror signal, is at an even greater distance from the receiver station than the mirror signal. This translates to an even wider subsurface illumination for the entire survey.

In OBS acquisition, Muijs et al. (2007) made an early attempt to image primary and free-surface multiples together. This requires the data to be decomposed into up-going and down-going constituents, followed by downward extrapolation and a 2D deconvolution-based imaging condition. While this technique is computationally efficient, its image contains crosstalk artifacts caused by interference from up-going and down-going waves not associated with the same subsurface reflector. In contrast to existing methods, we use least-squares reverse time migration to optimally combine structural information provided by each order of multiple reflection into images that are free from crosstalk.

It is the objective of the data processor to put everything together and not overload the interpreter with alternative images. In our earlier work (Wong et al., 2010), we have shown how the information in the primary and mirror signal can be combined to give one coherent image. In this paper, we focus on the improvement from performing LSRTM with the mirror signal and the subsequent higher-order multiples. Ultimately, we wish to perform joint inversion of the primaries and all the down-going surface related multiples. The rest of this paper is organized as follows. We first discuss the theory of linear least-squares inversion, we then apply the inversion scheme to a field survey located on the northern Cascadia continental margin.

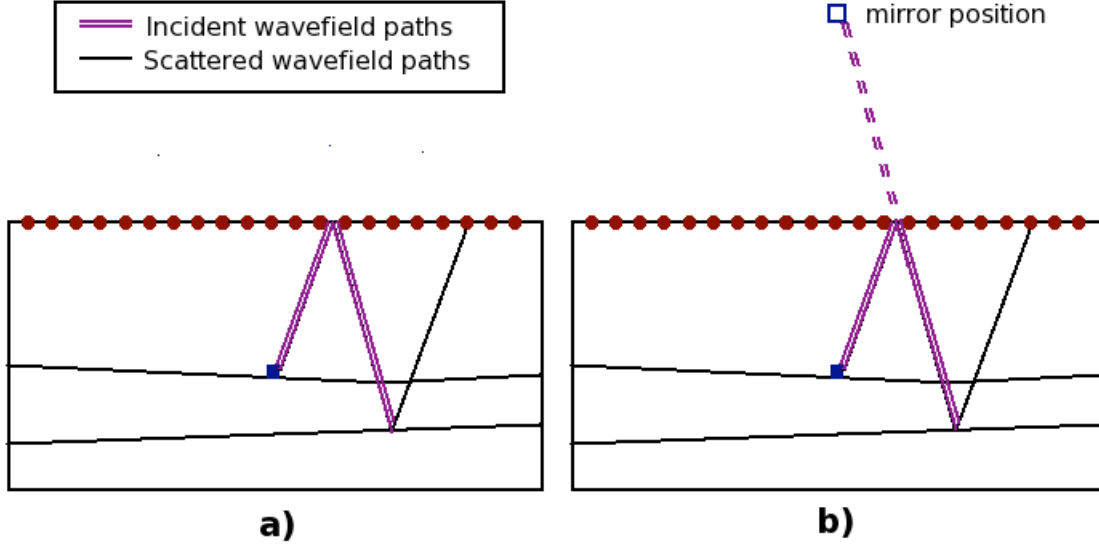


Figure 2: (a) The raypath of a mirror signal. (b) The raypath of the same signal in mirror imaging. The apparent position of the receiver is now at twice the ocean depth above the seabed. This assumes the sea surface is a perfect reflector. [NR]

THEORY

In general, pre-stack imaging of OBS acquisition is done in the common-receiver domain. For processing, the idea of reciprocity is applied, in which these common-receiver gather (CRG) are injected at the source location while the source wavelet is injected at the receiver location. We will first discuss how the migration operators are constructed. Afterwards, we will discuss how the least-squares migration problem is defined.

Conventional mirror imaging

The essence of conventional mirror imaging is to account for the kinematics of the mirror signal (Figure 2 (a)) by placing the receiver position at twice the ocean depth above the seabed. If the sea surface is a perfect reflector with a reflectivity of -1, then the simulated mirror migration path (Figure 2 (b)) will be equivalent to the mirror signal.

One advantage with mirror imaging is that the mirror's illumination aperture is much wider than that of the primary signal. Another advantage is that mirror imaging can be easily adapted to existing migration algorithms by changing the receiver position.

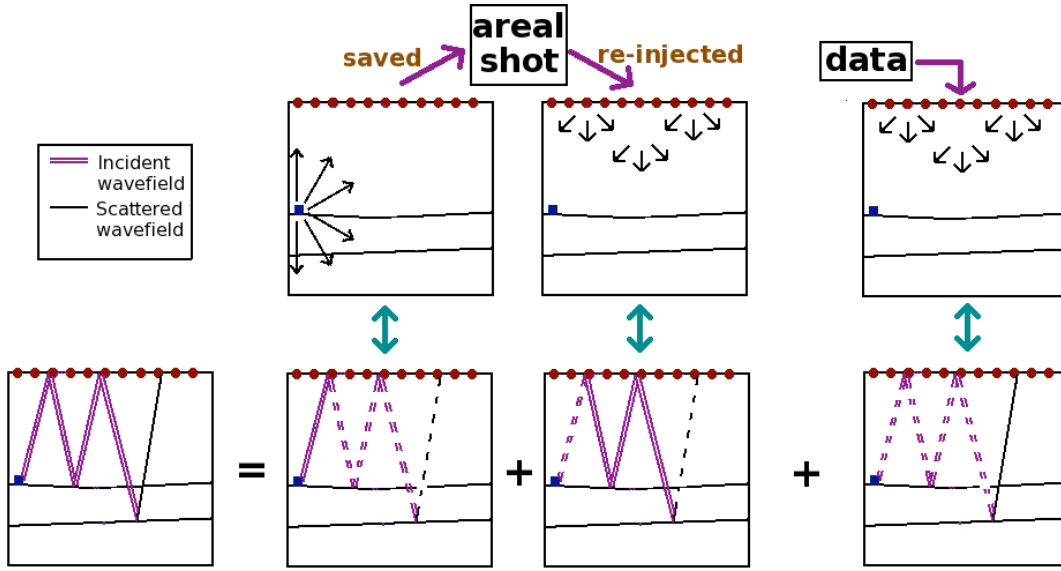


Figure 3: Illustration for the migration of the double-mirror signal. For the incident wavefield, an areal shot is pre-calculated to simulate the final down-going leg of the wave path. To generate the incident wavefield, the saved areal shot is re-injected at the sea-surface with a -1 factor. The re-injected signal is then allowed to travel back and forth in the water column using a reflecting top boundary and a well-defined velocity contrast at the sea-bottom. [NR]

Higher order mirror imaging

To image with higher-order multiples, we need to construct a migration operator that can account for the kinematics of the appropriate wave paths. To simulate the final down-going leg of the wave path, an areal shot is pre-calculated by first injecting the source wavelet at the receiver location, letting the wavefield propagate, and then capturing the signal at the sea surface (Figure 3). To generate the incident wavefield, the saved areal shot is re-injected at the sea-surface with a -1 factor. The re-injected signal is then allowed to travel back and forth in the water column using a reflecting top boundary and a well-defined velocity contrast at the sea-bottom. This algorithm can correctly simulate the wave paths traversed by the mirror signal, the double-mirror signal and even higher-order multiples.

Note that this technique does not migrate all orders of multiples. It only migrates surface-related multiples with a single reflection in the reflectivity model or with reflections in the acoustic modeling based on a sharp boundary in the velocity model.

Least-squares reverse time migration (LSRTM)

In OBS acquisition, pre-stack images are created from data in the common-receiver domain. This intrinsically requires that each trace in the CRG is de-signatured. In RTM, the migration image is a linear operator applied to the recorded data:

$$\mathbf{m}_{mig}(\mathbf{x}) = \sum_{\mathbf{x}_r, \mathbf{x}_s, \omega} \omega^2 f_s^*(\omega) G^*(\mathbf{x}_r, \mathbf{x}, \omega) G^*(\mathbf{x}, \mathbf{x}_s, \omega) d(\mathbf{x}_r, \mathbf{x}_s, \omega) \quad (1)$$

where ω is frequency, $m(\mathbf{x})$ represents the reflectivity at image point \mathbf{x} , $f_s(\omega)$ is the source waveform, and $G(\mathbf{x}_s, \mathbf{x}, \omega)$ is the Green's function that is the solution to the two-way acoustic constant-density equation. In practice, the Green's function is calculated using a finite-difference time-domain technique, and the multiplication in the frequency domain is replaced by a zero-lag cross-correlation in the time domain.

The difference between mirror imaging and higher-order mirror imaging lies within the incident wavefield, $U_s(\mathbf{x}_r, \mathbf{x}, \omega) = \omega^2 f_s(\omega) G(\mathbf{x}_r, \mathbf{x}, \omega)$, which is calculated differently to the method described in the previous two sub-sections.

To obtain a better reflectivity image, we go beyond migration by formulating the imaging problem as a least-squares inversion problem. The solution $m_{inv}(\mathbf{x})$ is obtained by minimizing the objective function $S(\mathbf{m})$, which is defined as the least-squares difference between the forward modeled data \mathbf{d}^{mod} and the recorded data \mathbf{d}^r .

$$S(\mathbf{m}) = \|\mathbf{d}^{mod} - \mathbf{d}\|_2 = \|\mathbf{Lm} - \mathbf{d}\|_2 \quad (2)$$

In least-squares reverse time migration (LSRTM), the forward modeled data is defined to be the Born approximation of the linearized acoustic wave equation:

$$d^{mod}(\mathbf{x}_r, \mathbf{x}_s, \omega) = \sum_{\mathbf{x}} U_s(\mathbf{x}_r, \mathbf{x}, \omega) G(\mathbf{x}, \mathbf{x}_s, \omega) \mathbf{m}(\mathbf{x}) \quad (3)$$

It is important to point out that the forward modeling operator \mathbf{L} is the adjoint of the reverse-time migration operator \mathbf{L}^T . Even for the case of modeling certain classes of surface-related multiples, the operator is still linear with respect to $m(\mathbf{x})$. This is because \mathbf{L} simulates only events that would interact with the model space once.

FIELD EXAMPLE

Next we present results of LSRTM on an OBS survey located at the northern Cascadia continental margin offshore of western Canada. The area is known to contain gas hydrates, which have a characteristic structure known as the bottom-simulating reflector (BSR), that marks the base of the hydrate stability zone. OBS data were collected along five parallel lines normal to the margin (Figure 4). Line spacing was 500 m with ten ocean-bottom seismometers deployed with 100 m spacing at a water depth of about 1300 m.

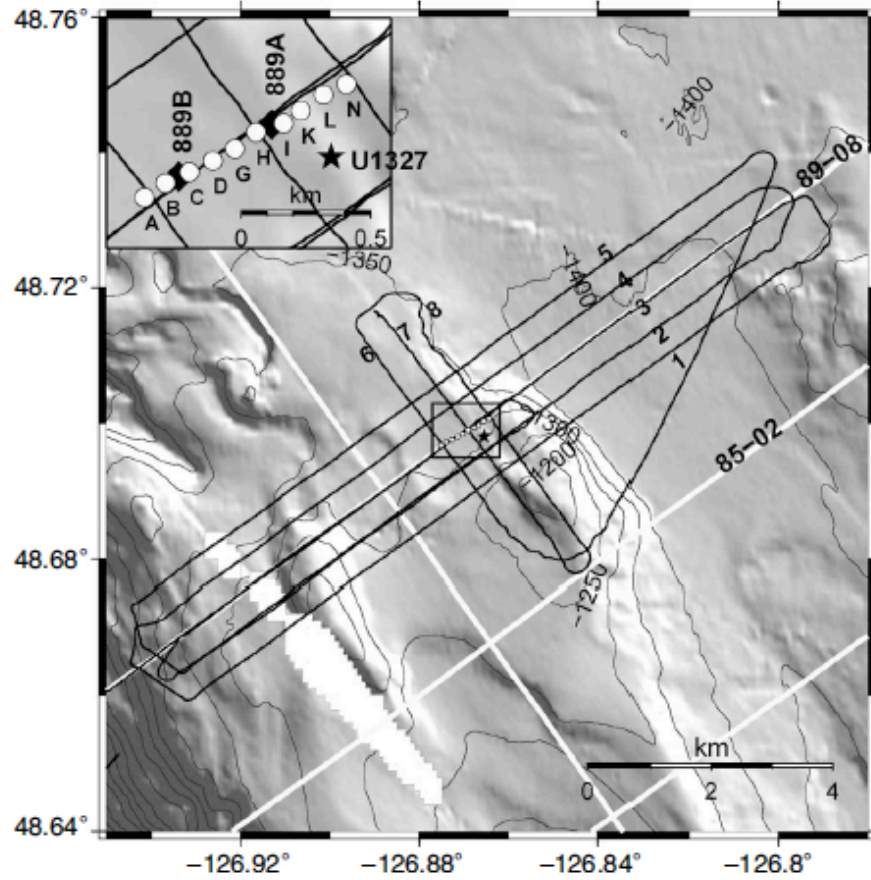


Figure 4: The geometry of the Northern Cascadia dataset. Ten ocean-bottom seismometers were deployed with 100 m spacing at a water depth of 1300 m. The shot line spacing was 500 m. [NR]

Pre-processing

In our 2D study, we extract a 2D shot line from directly above the OBS line. Following the processing step in Dash et al. (2009), we apply a gapped deconvolution with a 12-ms gap length and 300-ms filter length to suppress the source bubble. Out of the ten OBS receivers, only six were used for final imaging. These receivers were selected according to their data quality. Three receivers were rejected due to large tilt angles, and one receiver was rejected because it was saturated with noisy traces.

Since we only use the down-going wavefield, only acoustic separation above the seafloor is needed. We used the adaptive decomposition method of Schalkwijk et al. (1999).

These data are bandpassed between 5 and 45 Hz to avoid dispersion in the time-domain finite-difference calculation. These data before and after pre-processing are shown in Figure 5.

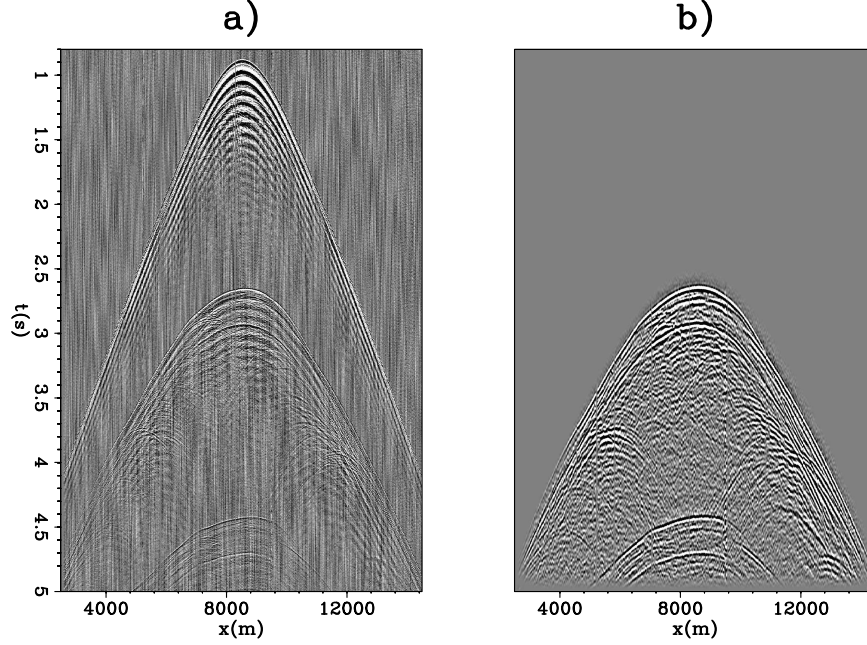


Figure 5: (a) A hydrophone common receiver gather (CRG) before pre-processing and (b) down-going data after pre-processing. [CR]

Figure 6 (a) shows the migration velocity used for our RTM and LSRTM. The velocity ranges from 1480m/s in the water column to 1820m/s in the sediment layer. The BSR lies at an approximate depth of 1500-m with a velocity inversion.

Migration and Inversion result

Figure 6 (b) shows the mirror-imaging RTM result. Overall, we can identify some migration artifacts associated with RTM, such as the high-amplitude low-frequency artifacts. The resolution is low, and the structural information below the BSR is generally difficult to identify.

Seismic inversion is an ill-posed problem. To prevent divergence to unrealistic solutions, we add an additional term to our objective function $S(\mathbf{m})$. In Nemeth et al. (1999); Ronen and Liner (2000), data weighting operators are used to remove the acquisition footprint by having zero weighting on regions corresponding to the acquisition gap. The overall fitting goal becomes

$$S(\mathbf{m}) = \|W(L\mathbf{m} - \mathbf{d})\|^2 + \epsilon^2 \|\mathbf{m}\|^2, \quad (4)$$

where \mathbf{W} is a diagonal data-weighting matrix, and ϵ tunes the level of damping in our objective function. The criterion for choosing ϵ is:

$$0.2 = \frac{\|\epsilon \mathbf{m}\|^2}{\|\mathbf{W}(L^T(\mathbf{d}^{mod} - \mathbf{d}))\|^2}. \quad (5)$$

In the first iteration, ϵ is defined by limiting the gradient contribution from the damping term to be 20% of the gradient contribution from the data fitting term. From experiments with both synthetic and field dataset, we found that this limit yields satisfactory results. For this dataset, the damping term alone seems to adequately regularize the inversion and yield a satisfactory result. For more complex survey regions, other regularization terms are needed to further constrain the inversion.

We apply LSRTM in two cases: (1) using the mirror-imaging operator (LSRTM-M) and (2) using the higher-order mirror-imaging operator (LSRTM-HM). The results after 10 iterations are shown in Figure 6 (c) and (d) respectively. Overall, the inversion images have higher resolution and fewer artifacts than the RTM image. However, there is not much difference between the two inversion results. One reason is that this dataset records only a small portion of the double-mirror signal. We expect the LSRTM-HM to provide substantial improvement in the case of a shallow-water dataset in which higher-order multiples overlap with lower order multiples. Comparing between RTM and LSRTM, we have identified two areas of improvement with some close-up sections in Figure 7:

1. Panels (a) and (b) show the RTM and LSRTM-M images from a section at $x=9400$ to 11600 m and $z=1350$ to 1700 m. We can see that the reflectors under the seabed are better resolved with LSRTM.
2. Panel (c) and (d) shows the RTM and LSRTM-M images from a section at $x=7500$ to 9500 m and $z=1400$ to 1750 m. For regions beneath the BSR, the amplitude of the true reflector has been strengthened, and we can now identify some structures there.

Convergence

We use the iterative conjugate direction method to minimize our objective function. Figure 8 (a) shows the value of the objective function over 20 iterations. The inversion converges nicely with the residuals dropping to 50% of the original value. It is important to point out that the final residual drop is problem dependent. In general, if the raw dataset contains a low signal-to-noise ratio, then the residual drop will be less. Figure 9 (a) shows a common receiver gather for this data set. After 20 iterations, the corresponding forward modeled data 9 (b) is able to capture most of the prominent signal in the data. The difference of the two yields the data residual shown in Figure 9 (c).

Another way to evaluate convergence is to study the ratio of the model residual over data residual. The model residual is defined to be applying the migration operator to the data residual at each iteration. (It is also called the gradient.) In Figure 8 (b), we can see that the ratio almost drops down to zero over iterations, which also indicates convergence.

DISCUSSION AND FUTURE WORK

Although our modeling operator in LSRTM-HM can generate higher-order surface-related multiples, we do not see major improvement in the inverted images. One reason is related to the fact that there is limited signal coming from the double-mirror event in our recorded data. This dataset only has recording up to five seconds which results in some truncation in the double-mirror signal. It will be interesting to test on datasets with either a longer recording time or a shallower sea bottom. Another reason is related to the constant density assumption in our ascoustic modeling. In Figure 9 (b), we can see that the double-mirror signal is generated in the modeling. However, its amplitude is significantly weaker than that in the field dataset (Figure 9 (a)). With a constant density propagation kernel, the higher-order multiples are generated solely from reflection off sharp contrasts/interfaces in the migration velocity model. For the Cascadia dataset, it turns out that the seabed's reflectivity is attributed significantly to the density contrast, which is not accounted for in our modeling. As a result, the velocity contrast alone does not account for the full reflectivity of the sea bottom. We are currently trying to match the correct reflectivity by implementing our LSRTM using the full ascoustic wave equation. That is, without the constant density assumption. Nearby well log data will be used to estimate the density contrast at the sea bottom.

The computational cost of LSRTM is higher than that of RTM, with a factor proportional to the number of iterations. For an OBS survey, such additional computational costs can still be affordable. This is because the number of pre-stack migrations needed equals the number of OBS receivers in the survey. The number of migration needed is substantially smaller than that in a towed-streamer survey. Recently, Dai et al. (2010) suggested using phase encoding in LSRTM, which can

reduce the computation substantially but introduces crosstalk into the image.

CONCLUSION

Although only 2D modeling and migration are used, we see improvements in the LSRTM image over conventional methods. Such improvements include suppression of migration artifacts, enhancement of amplitudes along true reflectors, and better resolution. We expect the extension to 3D will bring further improvements.

ACKNOWLEDGMENTS

The authors are thankful to Professor George Spence from the University of Victoria and the Dalhousie University for collection and permission to publish the OBS data. MW thanks Ranjan Dash for information and previous work on the field dataset. We thank the sponsors of the Stanford Exploration Project for their financial support.

REFERENCES

- Dai, W., C. Boonyasiriwat, and G. T. Schuster, 2010, 3d multi-source least-squares reverse time migration: SEG Expanded Abstracts, **29**, 3120–3124.
- Dash, R., G. Spence, R. Hyndman, S. Grion, Y. Wang, and S. Ronen, 2009, Wide-area imaging from obs multiples: Geophysics, **74**, Q41–Q47.
- Godfrey, R., P. Kristiansen, B. Armstrong, M. Cooper, and E. Thorogood, 1998, Imaging the foinaven ghost: 68th SEG Annual Meeting Expanded Abstracts, 1333–1335.
- Grion, S., R. Exley, M. Manin, X. Miao, A. Pica, Y. Wang, P. Granger, and S. Ronen, 2007, Mirror imaging of obs data: First Break, **25**, 37–42.
- Muijs, R., J. Robertsson, and K. Holliger, 2007, Prestack depth migration of primary and surface related multiple reflections: Part i - imaging: Geophysics, **72**, 59–69.
- Nemeth, T., W. Chengjun, and G. T. Schuster, 1999, Least-squares migration of incomplete reflection data: Geophysics, **64**, 208–221.
- Ronen, S., L. Comeaux, and J. Miao, 2005, Imaging downgoing waves from ocean bottom stations: 75th SEG Annual Meeting Expanded Abstracts, 963–966.
- Ronen, S. and C. Liner, 2000, Least-squares dmo and migration: Geophysics, **65**, 1364–1371.
- Schalkwijk, K. M., C. P. A. Wapenaar, and D. J. Verschuur, 1999, Application of two-step decomposition to multicomponent ocean bottom data: Theory and case study: Journal of Seismic Exploration, **8**, 261–278.
- Wang, Y., S. Grion, and R. Bale, 2009, What comes up must have gone down: the principle and application of up-down deconvolution for multiple attenuation of ocean bottom data: CSEG Recorder, **34**, 16–20.

Wong, M., B. Biondi, and S. Ronen, 2010, Joint least-squares inversion of up- and down-going signal for ocean bottom data sets: SEG Annual Meeting Expanded Abstracts, **29**, 2752–2756.

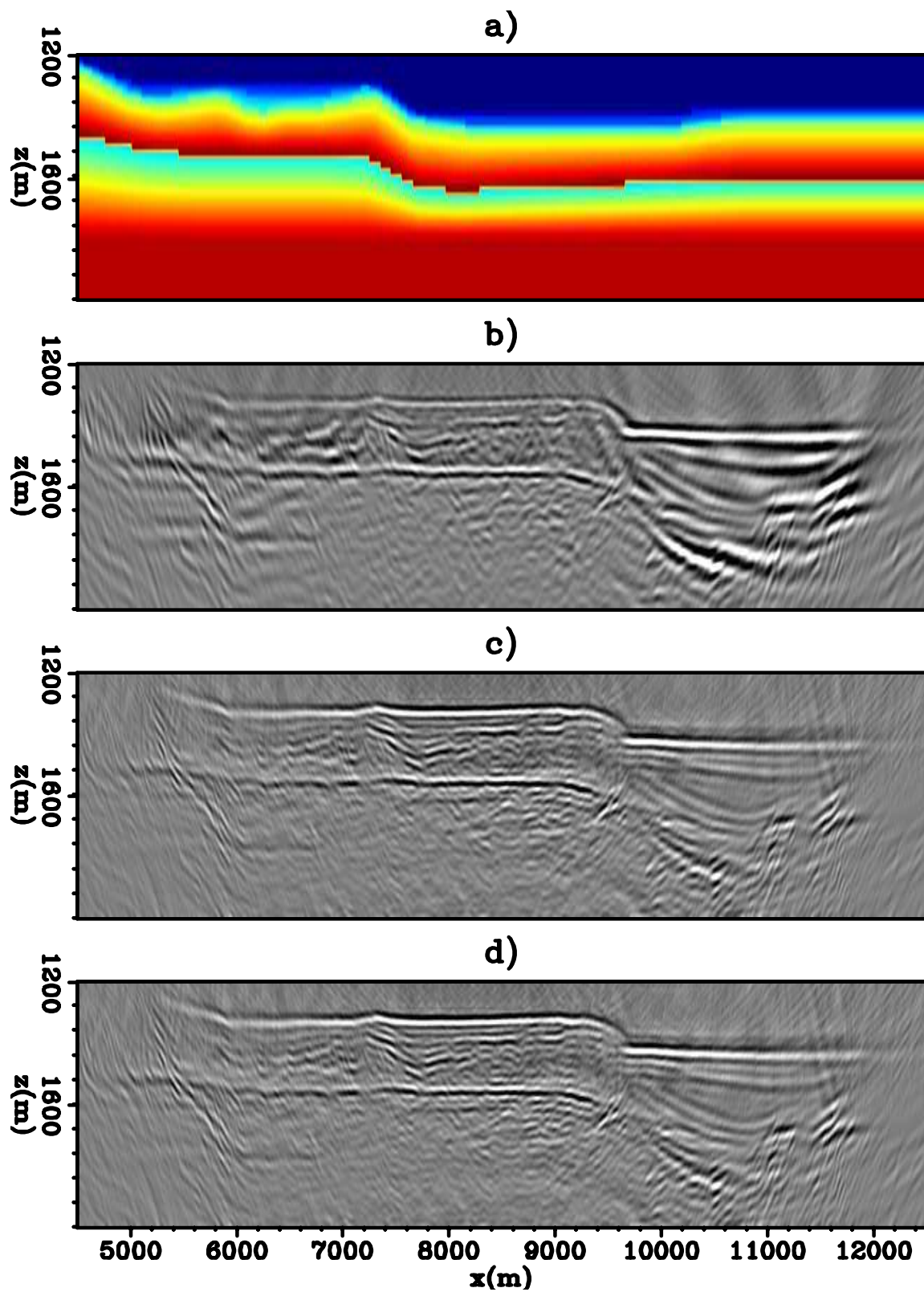


Figure 6: (a) Migration velocity model, (b) RTM image of the mirror signal, (c) LSRTM of the mirror signal (LSRTM-M), and (d) LSRTM of mirror and higher-order mirror signals (LSRTM-HM). [CR]

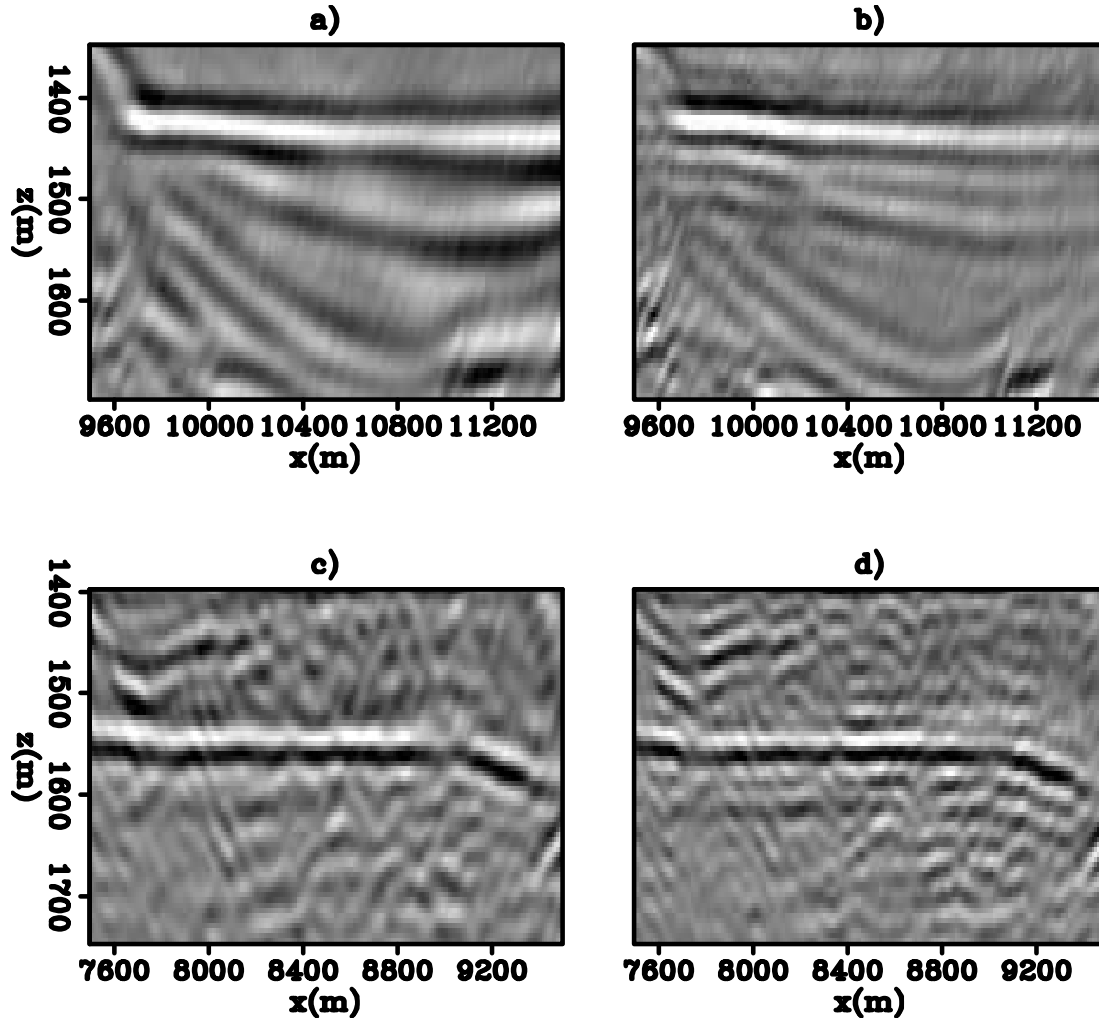


Figure 7: A section of the image cut from $x=9400-11600$ m and $z=1350-1700$ m after applying (a) RTM and (b) LSRTM-M. Another section of the image cut from $x=7500-9500$ m and $z=1400-1750$ m after applying (c) RTM and (d) LSRTM-M. [CR]

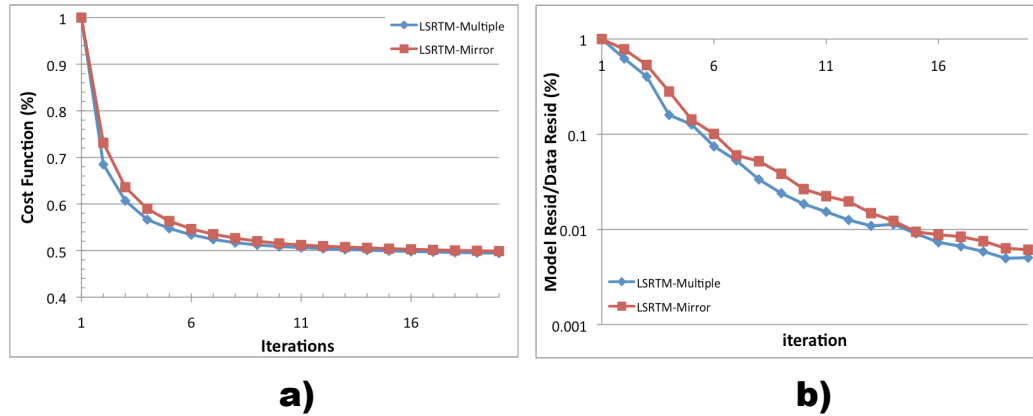


Figure 8: (a) Objective function over 20 iterations and (b) The ratio of model residual over data residual over 20 iterations (Note in log scale). [NR]

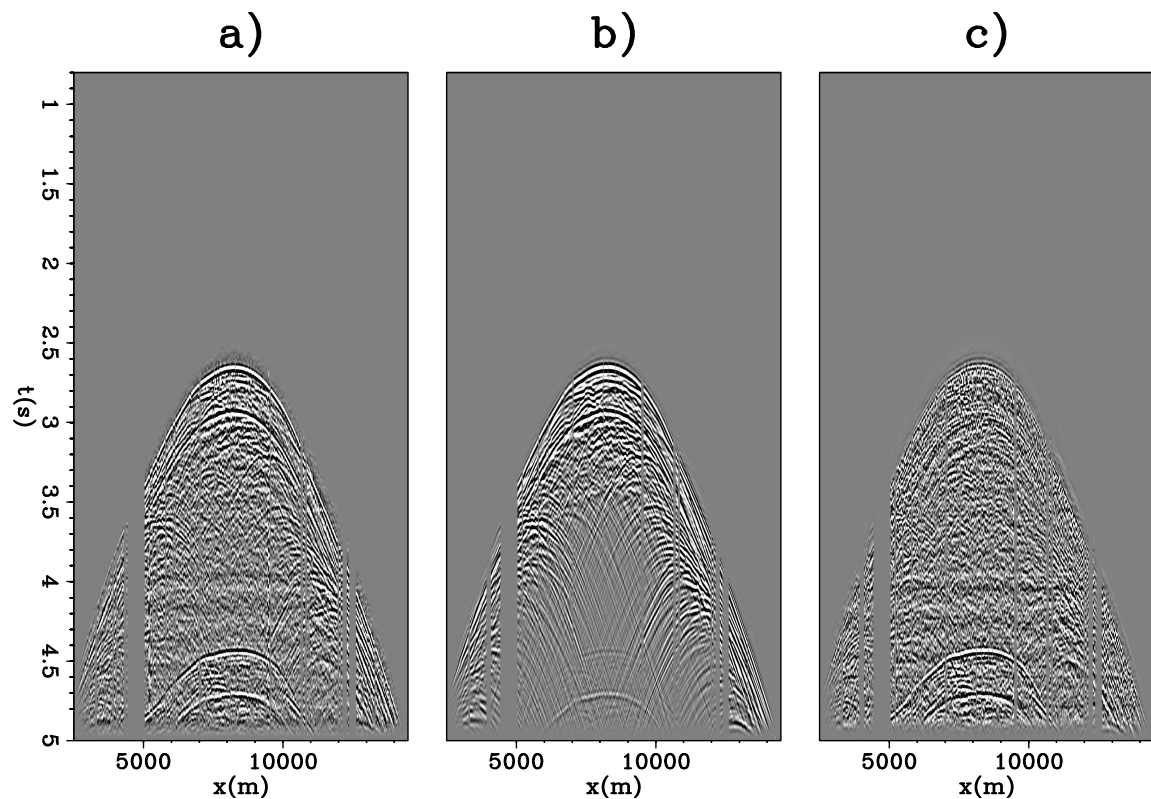


Figure 9: (a) A common receiver gather after pre-processing for one of the ocean-bottom seismometer, (b) the forward modeled data of the same gather using the LSRTM-M reflectivity image at the 20th iteration and (c) the data residual of the same gather at the 20th iteration, which is equivalent to the difference between (a) and (b). [CR]